🔓 **Open Access**

Decentered Gaussian Beam Pumped Highly Efficient Passively Q-Switched Microchip Laser for Controllable High-Order Transverse Modes

Ming-Ming Zhang
Hong-Sen He
Jun Dong

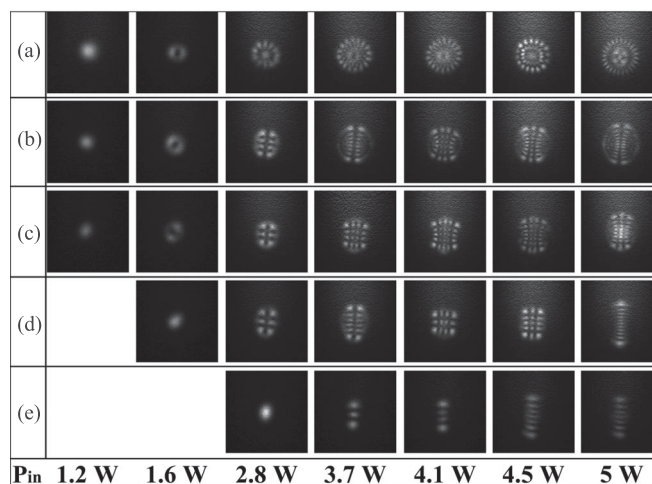# Decentered Gaussian Beam Pumped Highly Efficient Passively Q-Switched Microchip Laser for Controllable High-Order Transverse Modes

Ming-Ming Zhang, Hong-Sen He, and Jun Dong

Laboratory of Laser and Applied Photonics, Department of Electronics Engineering, School of Information Science and Engineering, Xiamen University, Xiamen 361005, China

Abstract: Versatile controllable high-order transverse laser modes have been generated in a decentered Gaussian beam (DGB) pumped Cr^{4+}:YAG passively Q-switched (PQS) Nd:YAG microchip laser. The DGB has been formed by offsetting collimating lens away from the propagation direction of the pump light. Effects of the collimating lens offset distance on the beam profile and tilting angle of the DGB have been investigated experimentally and theoretically. A highly efficient and high repetition rate Laguerre–Gaussian (LG) mode PQS microchip laser is achieved when the ordinary Gaussian beam is used as the pump source. The Ince–Gaussian (IG) mode and Hermite–Gaussian (HG) mode lasers are obtained when the DGB is applied as the pump source. The IG mode laser is changed to an HG mode laser by increasing the offset distance of the collimating lens. Optical efficiencies above 41% respective to the absorbed pump power have been obtained in the DGB pumped LG and IG mode PQS Nd:YAG microchip laser. The nanosecond pulse width and peak power of over 4 kW has been achieved in DGB pumped PQS Nd:YAG microchip lasers for various high-order transverse modes. Our works on the DGB pumped PQS microchip laser for high-order transverse modes provide an effective and simple method for designing highly efficient, controllable LG, IG, and HG mode solid-state lasers.

Index Terms: Decentered Gaussian beam, transverse laser mode, microchip laser, passively Q-switched.

1. Introduction

Besides Laguerre-Gaussian (LG) modes in the circular cylindrical coordinate and Hermite-Gaussian (HG) modes in the Cartesian coordinate, Ince-Gaussian (IG) modes are exact solutions of the paraxial wave equation in elliptic cylindrical coordinate [1], [2]. These laser modes with varieties of shapes have received wide attention in optical trapping [3], [4], manipulating microscopic particles and biological cells [5], [6], and the formation of vortex beams and vortex array [7], [8]. IG modes can also be transformed into HG or LG modes when the ellipticity parameter tends to ∞ or to 0, respectively. LG, IG and HG laser beams have been generated in solid-state laser resonators [9]–[15], but these solid-state lasers only produce one kind of high order transverse modes by
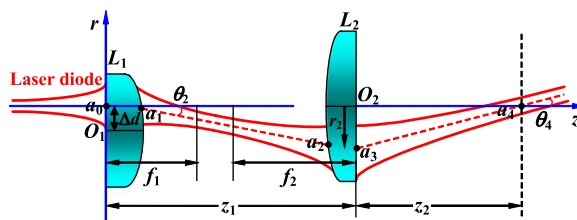
Fig. 1. Concept and propagation of decentered Gaussian beam (DGB), where L_1 and L_2 are the collimating and focus lens, respectively.

using these methods. If the three modes can be generated in one laser, further application of high order modes will be explored. The typical method for generating the three laser modes in the same solid-state laser is to use a liquid crystal spatial light modulator (SLM). A digital solid-state laser which produces LG, IG, HG and other high-order modes has been demonstrated [16] by using a phase-only reflective SLM as the rear cavity mirror. However, both the output power and the optical efficiency of the laser are quite low because of the additional losses from the SLM, compared to the conventional laser. Also the low damage threshold of the liquid crystal used for forming SLM limits the high power operation. A solid-state laser for transverse-mode selection has been demonstrated by unicursal fast-scanning pumping [17]. Simple LG, IG, and HG mode patterns have been obtained; however, the orders of the laser modes are very low. The finite pump beam area is the reason for the low order laser mode oscillation. And the complex experimental apparatus also limit the applications of the lasers. Recently, a method for oscillating LG, HG and IG modes in Cr^{4+}:YAG PQS Nd:YVO$_4$ microchip laser has been reported by moving the position of the Nd:YVO$_4$ crystal along the tilt direction of pump beam [18]. However, the LG, HG and IG mode lasers are very sensitive to the tilting angle of the pump beam, the LG or HG modes are difficult to oscillate when the tilting angle is too large or too small. The tilting angle of the pump beam has great effect on the performance of the microchip laser. The optical efficiency and peak power of the microchip laser is low. Therefore, PQS microchip lasers with controllable and high optical efficiency LG, IG, HG modes are still challenging and worthy of being investigated. The decentered Gaussian beam (DGB) [19], [20] has been realized by offsetting the center of the collimating lens from the beam axis. The DGB formed with laser diode does not only change the propagation direction, but also change the laser beam distribution. Compared with inserting wire and other optical devices in the laser resonator, the DGB pumped PQS microchip laser effectively reduces laser energy loss. Therefore, DGB should be an ideal pump source for PQS laser for generating various transverse modes. However, only the propagation of the DGB has been studied, and the DGB pumped solid-state laser has not been reported. The transverse modes formation in DGB pumped PQS microchip laser is worthy to being investigated.

In this paper, decentered Gaussian pump beam is formed by offsetting collimating lens from the beam axis of the laser diode. The beam profile and the titling angle of the DGB have been investigated as a function of the offset distance of the collimating lens away from propagation direction of the laser diode. The highly efficient DGB pumped Cr^{4+}:YAG PQS Nd:YAG microchip lasers for different transverse modes have been demonstrated for the first time to our best knowledge. Transverse laser modes, determined by the pumped area in the laser cavity, can be changed by using different tilted decentered Gaussian beams as pump sources. The highly efficient LG, IG, and HG mode PQS lasers with nanosecond pulse width have been achieved.

2. Propagation of Decentered Gaussian Beam

Two lenses L_1 and L_2 with different focal lengths are usually used to collimate and focus pump beam in a laser diode end-pumped microchip laser. The decentered Gaussian pump beam was obtained by offsetting collimating lens L_1 away from the propagating direction of the laser diode. Fig. 1 shows the concept of DGB through the collimating lens L_1, the focus lens L_2, and the

propagation of laser diode beam after offset collimating lens and focus lens. The incident pump beam shape from fiber-coupled laser diode is assumed to be Gaussian distribution. The offset distance of the collimating lens L_1 is Δd. The propagation of the DGB after collimating lens L_1 and focus lens L_2 is calculated with the help of the ABCD matrix. A Cartesian coordinate (r, z) is established for describing the propagation of DGB in Fig. 1. r and z are the radial direction and the propagation direction of pump beam, respectively. r_i and θ_i denote r-axis coordinate value and the incident angle of the pump beam at the point a_i, respectively. Here, we define when the angle θ_i is located above the z-axis, θ_i is positive and vice versa, θ_i is negative. The focal lengths of the collimating lens L_1 and the focus lens L_2 are f_1 and f_2, respectively. The center of the focus lens L_2 is along the propagation direction of the incident laser diode, e.g. the z-axis of laser diode (see Fig. 1).

When the center of the collimating lens L_1 is offset Δd away from the incident laser diode pump beam direction, the decentered beam is formed. $\Delta d > 0$ represents the center of the L_1 is located below the z-axis. To study on the pump beam propagation direction simple, we use the central ray of the pump beam to calculate the propagation properties of the DGB. With the help of the ABCD matrix [21] and without considering the thickness of the lenses, when the decentered pump beam propagates to the point a_2 of the focus lens L_2 after the L_1, these radial and angular parameters of central ray of the pump beam are related by the expression

$$\begin{bmatrix} r_2 + \Delta d \\ \theta_2 \end{bmatrix} = \begin{bmatrix} 1 & z_1 \\ 0 & 1 \end{bmatrix} \begin{bmatrix} 1 & 0 \\ -\frac{1}{f_1} & 1 \end{bmatrix} \begin{bmatrix} r_0 + \Delta d \\ \theta_0 \end{bmatrix} \tag{1}$$

where $r_0 = 0$, $\theta_0 = 0$, z_1 represents the distance between the two lenses.

Therefore, the distance and the angle between central ray and z-axis at the point a_2 can be expressed by

$$r_2 = (r_0 + \Delta d)\left(1 - \frac{z_1}{f_1}\right) + z_1\theta_0 - \Delta d \tag{2}$$

$$\theta_2 = \theta_0 - \frac{r_0 + \Delta d}{f_1} \tag{3}$$

where the absolute value of r_2 is less than the radius of L_2.

After beam propagating through the L_2, the central ray of pump beam at the point a_4 can be expressed by

$$\begin{bmatrix} r_4 \\ \theta_4 \end{bmatrix} = \begin{bmatrix} 1 & z_2 \\ 0 & 1 \end{bmatrix} \begin{bmatrix} 1 & 0 \\ -\frac{1}{f_2} & 1 \end{bmatrix} \begin{bmatrix} r_2 \\ \theta_2 \end{bmatrix} \tag{4}$$

where z_2 represents the distance between the L_2 and the rear surface of the laser crystal.

The distance and the angle between central ray and z-axis at the point a_4 can be expressed by the following formula:

$$r_4 = z_2\left(\theta_0 - \frac{r_0 + \Delta d}{f_1}\right) + \left(1 - \frac{z_2}{f_2}\right)\left[(r_0 + \Delta d)\left(1 - \frac{z_1}{f_1}\right) + z_1\theta_0 - \Delta d\right] \tag{5}$$

$$\theta_4 = \theta_0 - \frac{r_0 + \Delta d}{f_1} - \frac{(r_0 + \Delta d)\left(1 - \frac{z_1}{f_1}\right) + z_1\theta_0 - \Delta d}{f_2}. \tag{6}$$

The decentered pump beam with tilted angle of θ_4 and focused pump beam waist at a_4 position is formed by offsetting collimating lens L_1 and focused with L_2. According to the (6), the tilted angle θ_4 is a function of Δd, f_1, f_2, and z_1, and the tilted angle of the DGB, θ_4, increases linearly with the collimating lens offset distance, Δd, when the f_1, f_2 and z_1 are set. Theoretically, the propagating direction of the DGB, which exhibits a Gaussian intensity distribution on each cross section perpendicular to the z-axis, is linearly tilted with respect to the z-axis [19], [20]. However, in practice, the radius of curvature and thickness of the lens have great effect on the beam propagation.
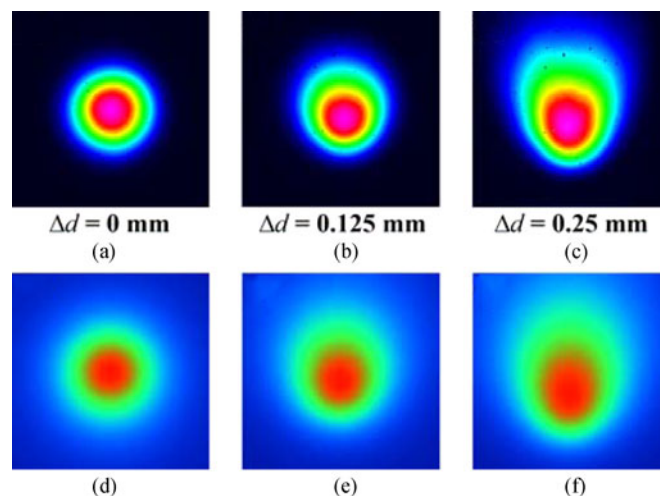
Fig. 2. Evolution of the experimentally observed intensity distributions of the DGB in the waist plane for different collimating lens offset distances ($\triangle d$) at incident pump power of 1.2 W. (a) $\triangle d = 0$ mm, (b) $\triangle d = 0.125$ mm, and (c) $\triangle d = 0.25$ mm. The focal lengths of the collimating lens (L_1) and focus lens (L_2) are 8 mm and 30 mm, respectively. The separation of the collimating lens and focus lens (z_1) is 165 mm. (d)–(f) are the theoretically simulated laser intensity distribution of the DGB at $\triangle d = 0$ mm, 0.125 mm, and 0.25 mm, respectively.

In order to verify the fidelity of the tilted angle of the DGB and the spatial distribution of the DGB as a function of the collimating lens offset distance, we set up an experiment according to the formation of the DGB in Fig. 1. A 808 nm fiber coupled laser diode was used as a light source. Two plane-convex lenses with focal lengths of $f_1 = 8$ mm, $f_2 = 30$ mm were used as the collimating lens and focus lens. The separation of two lenses was 165 mm.

The intensity distribution of the DGB was measured with a beam profiler at the waist $z = z_1 + z_2$ plane (as shown in Fig. 1). Some typical experimentally obtained laser beam profiles of the DGB in the waist plane for different offset distances of the collimating lens at the incident pump power of 1.2 W are shown in Fig. 2(a)–(c). The intensity distribution of the laser beam after optics coupling system was a circularly symmetric Gaussian profile at $\triangle d = 0$, as shown in Fig. 2(a). When the collimating lens offset distance $\triangle d$ was set to 0.125 mm, the tilted angle θ_4 of focused DGB was measured to be 4°, and the intensity distribution of the DGB was changed to be ellipse, as shown in Fig. 2(b). The peak was shifted away from the center axis of the laser diode beam direction. Further increasing the offset distance $\triangle d$ to 0.25 mm, the tilted angle θ_4 was further increased to 8°, and the pump beam shape was further elongated, as shown in Fig. 2(c). This non-Gaussian distribution of the DGB was formed to break the symmetry of the cavity, which forced the laser to oscillate in IG and HG modes. The intensity distribution of the DGB at different collimating lens offset distances was calculated with Zemax software by taking account into the radius of curvature and thickness of the lens. And the calculated intensity distributions of the DGB at $z = z_1 + z_2$ plane for $\triangle d = 0$, 0.125 and 0.25 mm were shown in Fig. 2(d)–(f), respectively. The focal lengths of the collimating lens and focus lens, $f_1 = 8$ mm, $f_2 = 30$ mm and the distance between two lenses of 165 mm were used in the calculations. The calculated intensity distributions of the DGBs at different collimating lens offset distance agreed well with the experimental measured beam profiles.

The tilted angle θ_4 of focused light beam was measured at different offset distance of the collimating lens ($\triangle d$). Fig. 3 shows the change of the tilted angle, θ_4, with the offset distance of the collimating lens in light propagation experiment. The tilted angle of the focused DGB increases linearly with the offset distance $\triangle d$. The variation of the tilted angle of focused DGB with the offset distance of the collimating lens $\triangle d$ was also calculated according to (6). The theoretically calculated tilted angle, θ_4, at different offset distance of the collimating lens is in good agreement with the experimental data, as shown in Fig. 3.
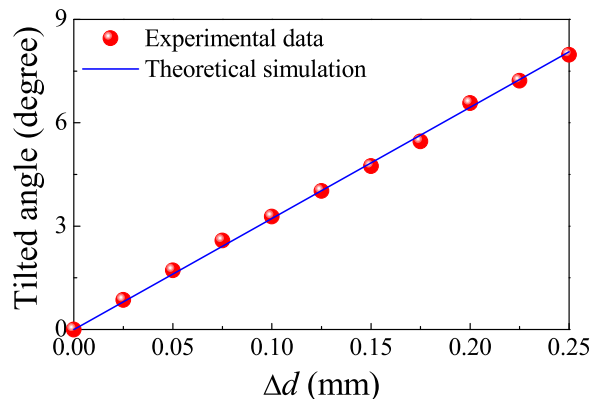
Fig. 3. Experimental results of the tilted beam angle (θ_4) at different offset distance of the collimating lens ($\triangle d$). The solid line is the theoretical calculation of the tilted angle of incident pump beam θ_4 with the $\triangle d$.
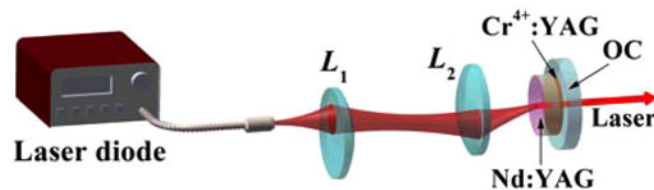

Fig. 4. Experiment setup of DGB pumped PQS Nd:YAG microchip laser. L_1 and L_2 are collimating and focus lenses, respectively. OC is the output coupler.

When decentered pump beam with a tilted angle is incident on the laser crystal, the pump power distribution inside the laser crystal is elliptical-like. The elliptical pump power intensity distribution forcing the PQS laser to oscillate at different laser strongly relies on the incident tilting angle and the shape of the pump beam. When an ordinary Gaussian beam was used as the pump source, as shown in Fig. 2(a), the pumped area was circularly symmetric. Therefore, the laser mode area was circular. Therefore, the LG modes oscillated in the PQS microchip laser owing to good beam matching. When a DGB with a small tilted angle was used as the pump source, as shown in Fig. 2(b), a small elliptical-like laser beam occurred within the elliptical-like pumped area. The symmetry of the laser cavity was broken and the laser was forced to oscillate in IG laser modes. When the incident tilted angle of the DGB was further increased, the pump area and laser mode area were elongated. The symmetry of the plane-parallel cavity was further broken with the elongated elliptical-like distribution of the inversion population inside the gain medium (as shown in Fig. 2(c)). The laser mode was not matched well with the pump beam area. In addition, the nonlinear absorption of the saturable absorber in PQS microchip laser further enhanced the asymmetrical saturated inversion population distribution. Therefore, the PQS Nd:YAG microchip laser oscillated in HG modes under a large tilting angle DGB pumping.

In general, the pump power intensity distribution and the tilted angle of the DGB incident on the surface of laser crystal were carefully chosen to control the laser modes generated in DGB pumped PQS microchip lasers.

3. Experiments

By applying a DGB as a pump source to change the incident tilted angle and pump beam area, we built a PQS Nd:YAG microchip laser for controllable high order transverse modes. Fig. 4 shows the DGB pumped Cr^{4+}:YAG PQS Nd:YAG microchip laser for various high order LG, IG, and HG
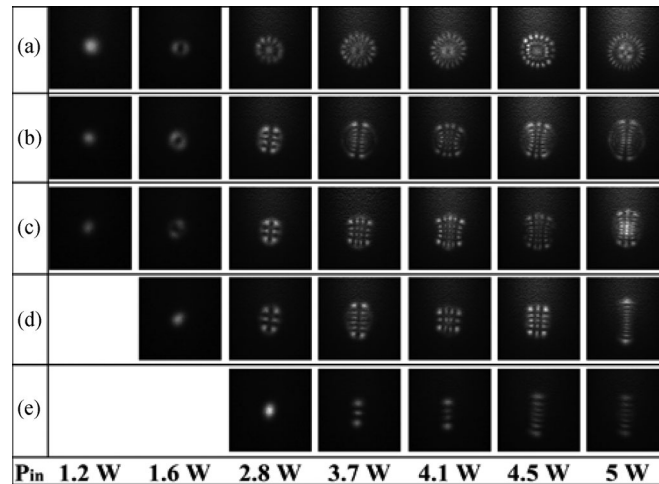
Fig. 5. Evolution of the experimentally observed transverse modes distribution of PQS Nd:YAG microchip laser with the incident pump power for different offset distance of collimating lens. (a) $\Delta d = 0$, (b) $\Delta d = 0.125$ mm, (c) $\Delta d = 0.25$ mm, (d) $\Delta d = 0.375$ mm, and (e) $\Delta d = 0.5$ mm.

transverse modes. The pump source was an 808 nm fiber-coupled laser diode (numerical aperture NA = 0.22, core diameter D = 400 μm). Two plane-convex lenses with the same focal length $f_1 = f_2 = 8$ mm were used to collimate and focus the pump beam from the fiber-coupled laser diode. The distance between two lenses was 70 mm. The collimating lens was offset away from the propagation direction of the laser diode to form a decentered Gaussian pump beam. The focus spot diameter was measured to be approximately 160 μm. The collimating lens was offset by 0, 0.125, 0.25, 0.375, and 0.5 mm, the corresponding tilted angle between the propagation direction of the decentered pump beam and normal direction of the surface of the laser crystal was approximately 0°, 6.9°, 13.9°, 20.8° and 27.8°, respectively. The microchip laser head was formed by sandwiching a thin piece of Cr^{4+}:YAG crystal between the Nd:YAG crystal and a plane-parallel output coupler (OC). The active medium was a 1.8 mm-thick, 1 at.% doped Nd:YAG thin crystal. The Nd:YAG surface facing pump source was coated with anti-reflection (AR) at the pump wavelength ($\lambda_p = 808$ nm) and high reflected (HR) at the lasing wavelength ($\lambda_l = 1064$ nm) to serve as the rear cavity mirror of this resonator. The intracavity loss was further reduced by coating AR at the lasing wavelength on other surface of the active medium. One uncoated 0.5 mm-thick Cr^{4+}:YAG crystal (initial transmission $T_0 = 95\%$) acted as the saturable absorber (SA). A 2-mm-thick K9 mirror with reflection of 95% at the lasing wavelength was used as OC. The cavity length was 2.3 mm. The laser was worked stably at ambient temperature. A beam profile (Thorlabs BC106-VIS CCD) was used to monitor and record the output laser transverse mode distribution. An InGaAs photodiode and a 6-GHz oscilloscope were used to detect the output laser pulse characteristics.

4. Results and Discussion

Fig. 5 shows the evolution of the experimentally observed transverse modes distribution of DBG end-pumped PQS Nd:YAG microchip laser with the incident pump power (P_{in}) for different offset distance of the collimating lens, and their corresponding numerically reconstructed laser mode distributions calculated by using LG, IG and HG mode expressions are shown in Fig. 6. The laser mode becomes more complex with increasing P_{in} for different collimating lens offset distance. In the case of normal incident of the pump beam on the laser crystal ($\Delta d = 0$), the PQS laser exhibited LG modes oscillation, as shown in Fig. 5(a). The LG mode number increases with the P_{in}. When P_{in} was less than 2 W, there was only one LG mode oscillating in the PQS microchip laser, e.g., TEM_{00} mode laser at 1.2 W and $LG_{0,1}$ mode laser at 1.6 W. When P_{in} was large than 2 W, two
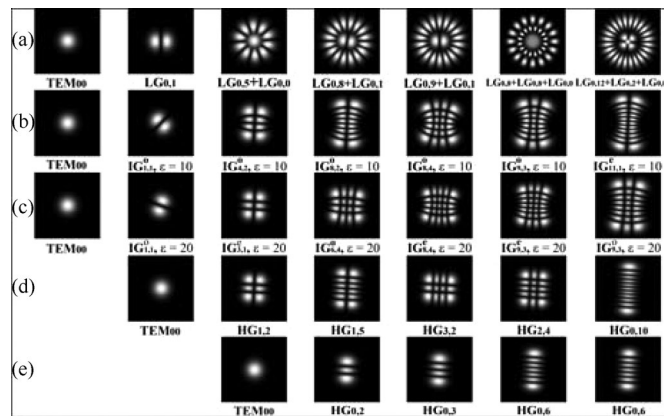
Fig. 6. Numerically reconstructed transverse mode distributions observed in PQS Nd:YAG microchip laser for different offset distance of the collimating lens by using LG, IG, and HG mode expressions. (a) $\Delta d = 0$, (b) $\Delta d = 0.125$ mm, (c) $\Delta d = 0.25$ mm, (d) $\Delta d = 0.375$ mm, and (e) $\Delta d = 0.5$ mm, which are corresponding to these transverse modes experimentally observed in Fig. 5.

LG modes oscillated simultaneously in the resonator such as $LG_{0,5} + LG_{0,0}$ modes at 2.8 W, $LG_{0,8} + LG_{0,1}$ modes at 3.7 W, and $LG_{0,9} + LG_{0,1}$ at 4.1 W. Three LG modes oscillated simultaneously when P_{in} was higher than 4.3 W, for example $LG_{0,8} + LG_{0,8} + LG_{0,0}$ at 4.5 W, $LG_{0,12} + LG_{0,2} + LG_{0,0}$ at 5 W. The two or three LG modes oscillation simultaneously was attributed to the large gain area in the laser crystal with the increase of the P_{in}, which made the high order LG modes oscillate. The LG mode oscillation of PQS microchip laser was kept when the collimating lens offset distance was slightly increased. Although the pump beam area was slightly changed away from Gaussian distribution with increasing the Δd, the laser mode area with sufficient inversion population was still maintained for LG mode oscillation for different P_{in}. The LG modes kept oscillation in PQS Nd:YAG microchip laser under DGB pumping when the Δd was less than 0.06 mm.

When the collimating lens was moved along the r-axis and positioned between 0.06 mm to 0.35 mm, the deformed pump beam area inside the laser crystal made the PQS Nd:YAG microchip laser oscillate in IG modes. The IG mode oscillation was caused by breaking the symmetry of gain distribution in the cavity when the tilted pump beam was applied at $\Delta d > 0.06$ mm. The elliptical pump beam inside the Nd:YAG crystal was still in good mode matching with the IG mode laser beam. When $\Delta d = 0.125$ mm, the IG modes with ellipticity parameter $\varepsilon = 10$ were obtained in the laser cavity, as shown in Fig. 5(b). The $TEM_{0,0}$ laser oscillated when the P_{in} was in the range from 0.9 W to 1.5 W. The IG modes oscillated when the P_{in} was higher than 1.5 W. The number of the IG mode increased with the P_{in}. $IG_{1,1}^{o}$ mode oscillated at $P_{in} = 1.6$ W. The $IG_{4,2}^{o}$ mode oscillated at $P_{in} = 2.8$ W. Further increasing the P_{in} to 3.7 W, the $IG_{8,2}^{o}$ mode oscillated. The $IG_{8,4}^{o}$ mode oscillated at $P_{in} = 4.1$ W. The $IG_{9,3}^{o}$ and the $IG_{11,1}^{e}$ modes were obtained when the P_{in} were 4.5 W and 5 W, respectively. When $\Delta d = 0.25$ mm, the IG modes with ellipticity parameter $\varepsilon = 20$ were obtained in the laser cavity, as shown in Fig. 5(c). The $TEM_{0,0}$ mode laser was kept when the P_{in} was less than 1.5 W. The IG modes oscillated when the P_{in} was higher than 1.5 W. The $IG_{1,1}^{o}$, $IG_{3,1}^{e}$, $IG_{6,4}^{o}$, $IG_{8,4}^{e}$, $IG_{9,3}^{e}$, and $IG_{9,3}^{o}$ modes were obtained depending on the applied P_{in}.

When the offset distance of the collimating lens was larger than 0.35 mm, the pump beam area was further deformed and enlarged. However, because the pump power intensity decreases with the enlarged pump beam area, only those pump area with sufficient inversion population can support laser oscillation and the HG modes were generated in the resonator, as shown in Fig. 5(d)–(e). The $TEM_{0,0}$, $HG_{1,2}$, $HG_{1,5}$, $HG_{3,2}$, $HG_{2,4}$ and $HG_{0,10}$ have been obtained depending on the P_{in} at $\Delta d = 0.375$ mm, as shown in Fig. 5(d). Especially, only $HG_{0,n}$ modes oscillated in the cavity when Δd was larger than 0.45 mm. The $TEM_{0,0}$, $HG_{0,2}$, $HG_{0,3}$, and $HG_{0,6}$ laser modes were obtained depending on the P_{in} for $\Delta d = 0.5$ mm.
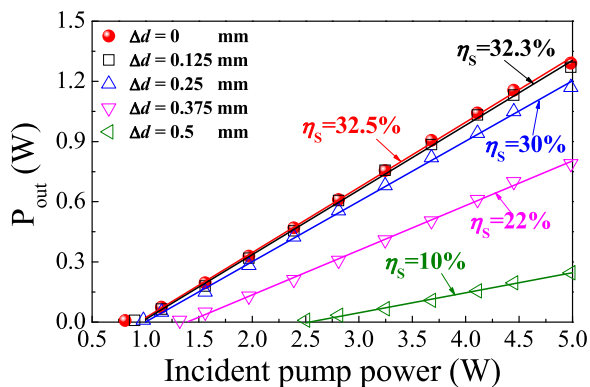
Fig. 7. Average output power (P_{out}) of DGB pumped high order transverse mode PQS microchip laser vs. P_{in} for different offset distance of the collimating lens $\triangle d$. The solid lines show linearly fitting of the experimental data.

As shown in Figs. 5 and 6, the ellipticity parameter of the laser mode increases from $\varepsilon = 0$ for LG laser mode to $\varepsilon = \infty$ for HG laser mode with increasing of the $\triangle d$. This is mainly attributed to the intensity profile of pump area elongating along the r-axis with the $\triangle d$ increasing. The change of the deformed pump beam area with the collimating lens offset distance $\triangle d$ and the mode matching between pump beam and laser beam are the main factors for generating high order mode laser. Various controllable transverse modes were generated in the PQS microchip laser depending on the P_{in} by applying the DGB with different offset distance of the collimating lens.

Fig. 7 shows the average output power (P_{out}) of PQS Nd:YAG microchip laser as a function of P_{in} for different offset distance of the collimating lens, $\triangle d$. When the focused pump beam was normally incident on the laser crystal, the laser exhibited LG mode oscillation. The pump power threshold was 0.81 W for $\triangle d = 0$. The pump power threshold increased with $\triangle d$, and the pump power thresholds were 0.9, 0.98, 1.32 and 2.5 W for $\triangle d = 0.125$, 0.25, 0.375 and 0.5 mm, respectively. The increase of the pump power threshold with the collimating lens offset distance $\triangle d$ is caused by the deformation of the pump beam and the mode mismatch between pump beam and laser beam. The P_{out} increased linearly with the P_{in} for different $\triangle d$. Meanwhile, the slope efficiency decreased with the $\triangle d$. Highest slope efficiency of 32.5% was achieved at $\triangle d = 0$. With the collimating lens offset distance was successively increased to 0.125, 0.25, 0.375 and 0.5 mm, the slope efficiency were 32.3%, 30%, 22% and 10%, respectively. Maximum P_{out} of 1.29 W was achieved for LG mode laser at $P_{in} = 5$ W. The P_{out} decreased with the $\triangle d$ for the same P_{in}. Maximum P_{out} of 1.27 W was obtained for IG mode laser at $\triangle d = 0.125$ mm when the P_{in} was 5 W. HG mode laser with maximum P_{out} of 0.79 W was achieved at $\triangle d = 0.375$ mm and $P_{in} = 5$ W.

When the P_{in} of 5 W is applied in the DGB pumped PQS Nd:YAG microchip laser, the average output power (P_{out}) and optical-to-optical efficiency (η_{O-O}) of PQS Nd:YAG microchip laser as a function of the collimating lens offset distance are shown in Fig. 8. The P_{out} decreases with the collimating lens offset distance. The P_{out} decreases slowly with the $\triangle d$ when the $\triangle d$ is less than 0.25 mm, and then decreases rapidly with the $\triangle d$ when the $\triangle d$ is larger than 0.25 mm. The η_{O-O}, the ratio of the P_{out} to the P_{in}, firstly decreases slowly and then decreases rapidly with the $\triangle d$ when the $\triangle d$ is larger than 0.25 mm. The η_{O-O} of 26% for LG mode laser at $\triangle d = 0$ is decreased to 5% for $HG_{0,n}$ at $\triangle d = 0.5$ mm. IG mode laser with the highest optical efficiency of 25.5% was achieved at $\triangle d = 0.125$ mm. HG mode laser with the highest optical efficiency of 15.8% was achieved at $\triangle d = 0.375$ mm. This may be attributed to the pump area increases slowly at first and then increases rapidly with increasing offset distance. The η_{O-O} of PQS microchip laser depends on the pump power intensity. The pump power intensity is decreased owing to an increase of the pump beam area with the offset distance under the same P_{in}. Therefore, the η_{O-O} of the PQS Nd:YAG microchip laser decreases with the collimating lens offset distance.
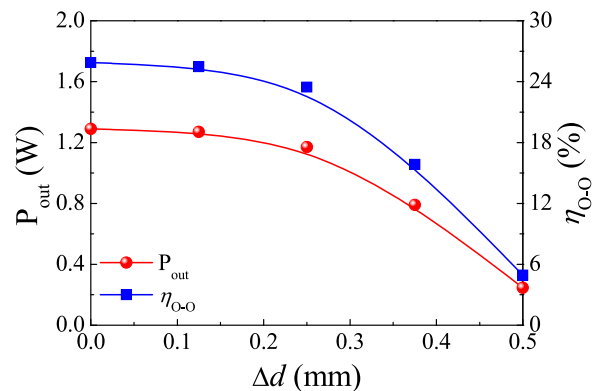
Fig. 8. Average output power (P_{out}) and optical-to-optical efficiency (η_{O-O}) of PQS microchip laser as a function of the offset distance of the collimating lens $\triangle d$ at incident pump power of 5 W. The symbols indicate the experimental data, the solid lines show the variation tendency of the experimental data.

For accuracy of evaluating the optical conversion efficiency of DGB pumped PQS Nd:YAG microchip laser for various transverse modes, we measured the absorbed pump power (P_{abs}) of Nd:YAG crystal. The η_{O-O} respect to the P_{abs} is calculated. The highest optical efficiency with respect to P_{abs} are 42.5% for LG mode laser and 41.6% for IG mode laser, which is about 25% higher than that obtained in Cr,Nd:YAG microchip lasers under tilted laser diode pumping [13]. Therefore, the highest optical efficiency with respect to the P_{abs} has been achieved in the PQS Nd:YAG microchip laser for LG and IG modes to our best knowledge. Compared to laser diode tilted pumped Cr,Nd:YAG microchip laser [13], DGB pumped PQS microchip laser constructed with separated Nd:YAG crystal and Cr^{4+}:YAG crystal as the gain medium and SA. The separation of Nd:YAG crystal and Cr^{4+}:YAG crystal dramatically reduces the defects in Cr,Nd:YAG crystal; therefore, the laser performance is dramatically enhanced. In addition, compare to two focus lenses with $f_1 = 8$ mm and $f_2 = 11$ mm focal length were used in the [13], two focus lenses with $f_1 = f_2 = 8$ mm focal length were used in our experiment also reduce the waist of the pump beam incident on the laser crystal for achieving high pump power intensity. Therefore, highly efficient, DGB pumped PQS Nd:YAG microchip laser for LG, IG and HG modes has been achieved. Compared with the conventional methods such as directly tilted pumping for generating high order transverse modes in laser diode pumped solid state laser, DGB pumped PQS microchip laser is more flexible and easy to accomplish. In general, there are two ways for achieving tilted pumping such as tilting pump sources or tilting laser cavities. However, these two ways have obvious disadvantages. When the pump source is tilted, the collimating and focusing system is tilted accordingly, which makes the laser system more complex and difficult to control the tilted angle. For the method of tilting the laser cavity, the laser output direction is changed, which is not suitable for the laser applications. The DGB pumped PQS microchip laser is easy and flexible to control the output transverse modes while keeps the output laser direction unchanged, which makes the laser more suitable for various applications.

Repetition rate and pulse width of DGB pumped PQS microchip laser as a function of the collimating lens offset distance ($\triangle d$) at $P_{in} = 5$ W are shown in Fig. 9. The repetition rate decreases with the $\triangle d$. The repetition rate of 68.8 kHz for LG mode laser at $\triangle d = 0$ decreases to 16.8 kHz for HG mode laser at $\triangle d = 0.5$ mm. IG mode laser with maximum repetition rate of 58.5 kHz was achieved at $\triangle d = 0.125$ mm. And HG mode laser with maximum repetition rate of 39 kHz was achieved at $\triangle d = 0.375$ mm. The pulse width is nearly kept constant with the P_{in} for different $\triangle d$. The pulse width increases slowly with the collimating lens offset distance ($\triangle d$) when the $\triangle d$ is less than 0.37 mm and then increases rapidly with further increasing of the $\triangle d$. The shortest laser pulse width of 3.5 ns was obtained at $\triangle d = 0$. For $\triangle d = 0.125, 0.25, 0.375$ and 0.5 mm, pulse width is about 4, 5.2, 7 and 15 ns, respectively. The increase of the laser pulse width with the $\triangle d$ is attributed
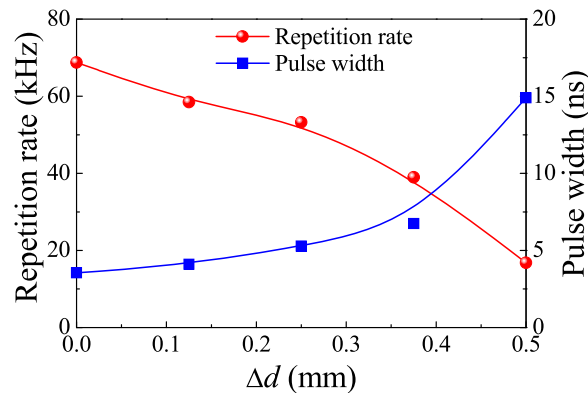
Fig. 9. Repetition rate and pulse width of DGB pumped PQS microchip laser as a function of the offset distance of the collimating lens $\triangle d$ at incident pump power of 5 W. The symbols indicate the experimental data, and the solid lines show the variation tendency of the experimental data.

Fig. 10. Pulse energy and peak power of DGB pumped PQS microchip laser as a function of the offset distance of the collimating lens $\triangle d$ at incident pump power of 5 W. The symbols indicate the experimental data, and the solid lines show the variation tendency of the experimental data.
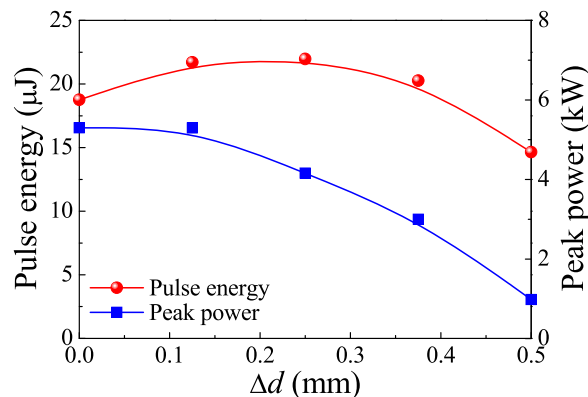
to the decrease of the pump power density. The pump beam area increases with the $\triangle d$, and the pump power intensity is decreased at the same P_{in}. The low intracavity laser intensity under low pump power intensity is not sufficient to bleach the SA, therefore establishing that a pulse needs more time at the same P_{in}.

Fig. 10 shows pulse energy and peak power of DGB pumped PQS microchip laser as a function of the collimating lens offset distance ($\triangle d$) at $P_{in} = 5\,W$. The pulse energy increases slowly with the $\triangle d$ when the $\triangle d$ is less than 0.25 mm and then decreases with further increasing of the $\triangle d$. There is an optimal $\triangle d$ for achieving highest pulse energy in DGB pumped PQS Nd:YAG microchip laser. The highest pulse energy of 22 μJ was achieved for IG mode laser at $\triangle d = 0.25$ mm. The pulse energy of PQS laser is proportional to the laser beam area [22], which is related to the pump beam area. The pump beam area increases with the $\triangle d$, so the possible laser beam area also increases with the $\triangle d$. However, the pump power intensity decreases with the $\triangle d$ at the same P_{in}. The inversion population excited in the laser gain medium is decreased and can not support large laser beam area, thus, there is a tradeoff between pump power intensity and pump beam area for achieving high energy output. When the DGB is incident normally on the laser crystal, the good mode matching is achieved, and the pump power intensity is sufficient to support laser oscillation. The pump power intensity is still sufficient to support laser oscillation by offsetting collimating lens, and laser beam area is still in good match with the pump beam area; therefore, the output energy of
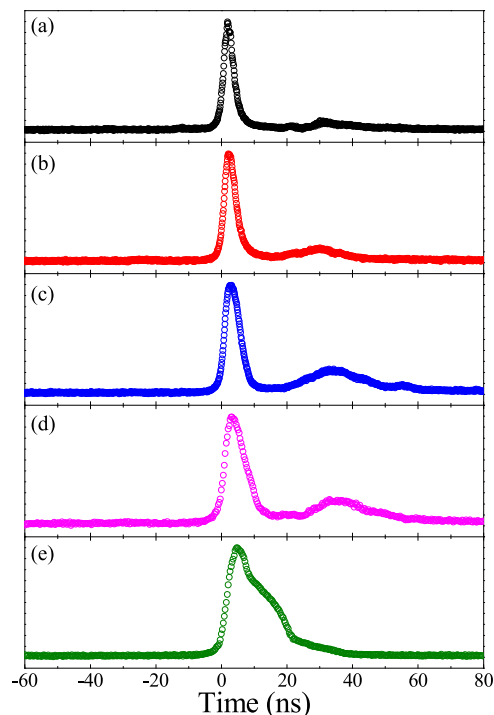
Fig. 11. Pulse profiles of DGB pumped high order transverse mode PQS microchip laser at P_{in} = 4.1 W for different offset distance of the collimating lens $\triangle d$. (a) $\triangle d = 0$, (b) $\triangle d = 0.125$ mm, (c) $\triangle d = 0.25$ mm, (d) $\triangle d = 0.375$ mm, and (e) $\triangle d = 0.5$ mm.

PQS microchip laser increases with the $\triangle d$. The laser beam area increases with the $\triangle d$; however, the pump power intensity is decreases with the $\triangle d$, and therefore, the output energy reaches a maximum value under the same P_{in}. The pump power intensity is not sufficient to support enlarged pump beam area to oscillate with further increasing $\triangle d$, therefore, the output energy decreases with further increasing $\triangle d$. Highest pulse energy of 22 μJ was achieved for IG modes in DGB pumped PQS Nd:YAG microchip laser at $\triangle d = 0.25$ mm. LG mode laser with the highest pulse energy of 18.8 μJ was achieved at $\triangle d = 0$ mm. HG mode laser with the highest pulse energy of 20.3 μJ was achieved at $\triangle d = 0.375$ mm.

The peak power is kept almost unchanged with the $\triangle d$ when the $\triangle d$ is less than 0.13 mm and then decreases with further increasing offset distance of the collimating lens ($\triangle d$), as shown in Fig. 10. The variation of the peak power with the $\triangle d$ is attributed to the increase of the pulse width with the $\triangle d$ and the variation of the pulse energy with the $\triangle d$. LG mode laser with highest peak power of 5.3 kW was achieved for $\triangle d = 0$ at $P_{in} = 5$ W. IG mode laser with highest peak power of 5.3 kW was obtained for $\triangle d = 0.125$ mm at $P_{in} = 5$ W. HG mode laser with highest peak power of 3 kW was achieved for $\triangle d = 0.375$ mm. The $HG_{0,6}$ mode laser with peak power of 1 kW was also achieved for $\triangle d = 0.5$ mm.

The collimating lens offset distance also has great effect on the pulse profiles for different high order transverse modes in DGB pumped PQS Nd:YAG microchip laser. Fig. 11 shows the typical pulse profiles of DGB pumped high order transverse mode PQS microchip laser for different offset distance of the collimating lens ($\triangle d$) at $P_{in} = 4.1$ W. The laser pulse with pulse width of 3.5 ns was obtained for high order LG mode PQS microchip laser. With increasing offset distance of the collimating lens, the pulse width is increased from 3.5 to 14.5 ns. A satellite pulse followed one main pulse at $\triangle d = 0.125$, 0.25 and 0.375 mm and the intensity of the satellite pulse increases with the $\triangle d$. Satellite pulse disappears and broaden pulse profile is observed at $\triangle d = 0.5$ mm. The pulse width of the PQS laser depends on the pump power intensity. Pump beam size has a great
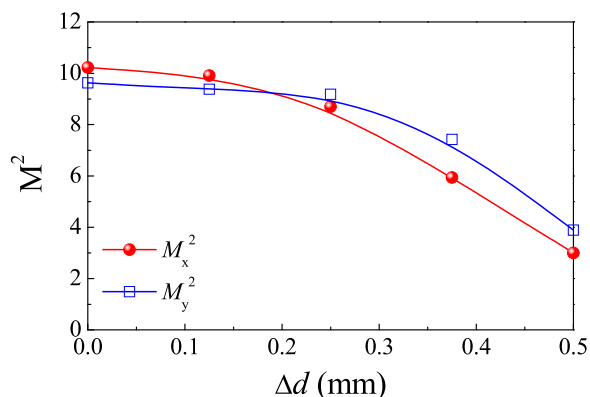
Fig. 12. Beam quality factor (M^2) of DGB pumped high order transverse mode PQS microchip laser as a function of $\triangle d$ at the incident pump power of 4.1 W. The solid lines are used to illustrate the variation of the M^2 with the $\triangle d$.

influence on the pulse width at the same P_{in} [23], and the pulse width increases with increasing pump beam size at the same P_{in} [18]. Pump area of DGB pumped PQS Nd:YAG microchip laser increases with increasing in the collimating lens offset distance at the same P_{in}, and the pump power intensity is decreased with the $\triangle d$. Therefore, the pulse width increases with $\triangle d$. The laser pulses with a satellite pulse at $\triangle d = 0.125$ mm, 0.25 mm, 0.375 mm and the broadened pulse profile at $\triangle d = 0.5$ mm are attributed to the deformation of the incident pump beam and decrease of the pump power intensity of DGB with increasing of the $\triangle d$. The laser pulse profiles are strongly affected by the pump power intensity and mode matching between pump beam and laser beam. The pump power intensity decreases with the collimating lens offset distance. The good mode matching is kept between pump and laser beam with the $\triangle d$ when the $\triangle d$ is less than 0.25 mm and then tends to become worsen with further increasing $\triangle d$. The single pulse at $\triangle d = 0$ is caused by the fully bleaching of the SA. The satellite pulses at $\triangle d > 0$ are caused by the high order mode oscillation within the larger laser area. The variation of the inversion population in the large pumped area causes the variation of the intracavity laser intensity, which induces the partially bleaching of the SA. Therefore, fully bleached SA causes a main pulse generation, and the partially bleaching of the SA induces a satellite pulse generation. When $\triangle d$ is increased from 0.125 mm to 0.25 mm, the pumped area is enlarged, and the laser area is also enlarged. Owing to the strong pump power intensity, the mode matching keeps still well between pump and laser beams, therefore, the enlarged laser beam area leads to the main pulse and satellite pulse energy increase with the $\triangle d$. When the $\triangle d$ increases from 0.25 mm to 0.375 mm, the pump beam area is increased with the $\triangle d$, and the pump power intensity is further decreased. The inversion population within the pump beam area can not support laser oscillate within the whole pumped area, therefore, the laser area is reduced, mode mismatch between pump and laser beams is getting worsened. Therefore, the pulse energy decreases with the $\triangle d$. The laser intensity in the cavity is still strong enough to continue enhance the oscillation of the satellite pulses. When the $\triangle d$ increases from 0.375 mm to 0.5 mm, there is a sharp decline in pump power intensity due to the rapid increase of the pumped area. Inversion population is insufficient to support satellite pulse oscillation. The change of the pulse profile with the $\triangle d$ is in good agreement with the variation of the pulse energy with the $\triangle d$, as shown in Fig. 10.

The beam quality factor (M^2) is an important parameter of the high order transverse mode PQS microchip laser for various applications. Therefore, the beam quality factors of various transverse modes PQS microchip lasers have been evaluated by measuring the beam waist at different positions along the propagation direction. Fig. 12 shows the variation of the M^2 for different transverse modes PQS Nd:YAG microchip lasers with the collimating lens offset distance at $P_{in} = 4.1$ W. The variation of the beam quality factor along horizontal and vertical directions (M_x^2 and M_y^2) is comparable. The beam quality factor M^2 decreases slowly with the $\triangle d$ when the $\triangle d$ is less than 0.25 mm

and then decrease rapidly when the $\triangle d$ is further increased. The M^2 is about 10 for LG modes when the $\triangle d$ is less than 0.06 mm. The M^2 keeps about 10 for IG modes laser. The M^2 decreases to 7.4 for $HG_{m,n}$ mode laser when the $\triangle d$ is increased to 0.375 mm. Further increasing $\triangle d$ to 0.5 mm, the M^2 for the $HG_{0,n}$ mode laser is decreased to 3.9. Owing to the high order transverse mode oscillation in DGB pumped PQS microchip laser at $P_{in} = 4.1$ W, the beam quality factor M^2 is relatively large compared to that of the fundamental mode laser. However, beam quality factor (M^2) less than 10 is the achievable excellent beam quality for various high order transverse modes PQS Nd:YAG microchip solid-state lasers. The improvement of the beam quality with the $\triangle d$ is attributed to the decrease of the transverse mode order. The beam quality factor of the high order transverse mode laser is proportional to the index of the transverse mode [24]. The pump power intensity is decreased with the $\triangle d$; therefore, the inversion population in the deformed pump beam area can not support higher order transverse mode oscillation. The mode number is decreased with the $\triangle d$. Thus, the beam quality factor is decreased with the $\triangle d$.

5. Conclusions

High beam quality PQS Nd:YAG microchip lasers for controllable high order LG, IG, and HG modes have been generated under DGB pumping. The decentered Gaussian pump beam is formed by offsetting collimating lens away from the beam axis of laser diode. The effects of the collimating lens offset distance on the focused pump beam profile and tilting angle have been studied theoretically and experimentally. The pump power distribution is deformed to elliptical and the tilting angle of the pump beam increases linearly with the collimating lens offset distance. Highly efficient high order LG, IG, and HG mode lasers have been achieved under DGB pumping depending on the offset distance of the collimating lens. The LG and IG modes lasers with optical efficiency of above 41% with respect to the absorbed pump power have been achieved in the PQS Nd:YAG microchip laser, which is the highest optical efficiency in the PQS Nd:YAG microchip laser to our knowledge. The controllable high order transverse mode PQS Nd:YAG microchip lasers with nanosecond pulse width and peak power of over 4 kW have been obtained. The decentered pump beam formed by offsetting collimating lens provides a more effective pump scheme for achieving high order LG, IG and HG modes in Cr^{4+}:YAG PQS Nd:YAG microchip laser. Our work on DGB pumped PQS microchip laser provides a novel method for designing highly efficient, controllable high order transverse mode lasers, which are more compact, robust, and have potential applications on vortex beam formation, quantum computation, and so on.

Acknowledgment

References

[1] M. A. Bandres and J. C. Gutiérrez-Vega, "Ince–Gaussian beams," *Opt. Lett.*, vol. 29, no. 2, pp. 144–146, Jan. 2004.
[2] M. A. Bandres and J. C. Gutiérrez-Vega, "Ince-Gaussian modes of the paraxial wave equation and stable resonators," *J. Opt. Soc. Amer. A, Opt. Image Sci. Vis.*, vol. 21, no. 5, pp. 873–880, May 2004.
[3] M. Woerdemann, C. Alpmann, M. Esseling, and C. Denz, "Advanced optical trapping by complex beam shaping," *Laser Photon. Rev.*, vol. 7, no. 6, pp. 839–854, Nov. 2013.
[4] M. Woerdemann, C. Alpmann, and C. Denz, "Optical assembly of microparticles into highly ordered structures using Ince-Gaussian beams," *Appl. Phys. Lett.*, vol. 98, no. 11, Mar. 2011, Art. no. 111101.
[5] S. Sato, M. Ishigure, and H. Inaba, "Optical trapping and rotational manipulation of microscopic particles and biological cells using higher-order mode Nd:YAG laser beams," *Electron. Lett.*, vol. 27, no. 20, pp. 1831–1832, Sep. 1991.
[6] R. Dasgupta, S. Ahlawat, R. S. Verma, and P. K. Gupta, "Optical orientation and rotation of trapped red blood cells with Laguerre-Gaussian mode," *Opt. Exp.*, vol. 19, no. 8, pp. 7680–7688, Apr. 2011.
[7] T. Ohtomo, S. C. Chu, and K. Otsuka, "Generation of vortex beams from lasers with controlled Hermite– and Ince–Gaussian modes," *Opt. Exp.*, vol. 16, no. 7, pp. 5082–5094, Mar. 2008.
[8] S. C. Chu, C. S. Yang, and K. Otsuka, "Vortex array laser beam generation from a Dove prism-embedded unbalanced Mach–Zehnder interferometer," *Opt. Exp.*, vol. 16, no. 24, pp. 19934–19949, Nov. 2008.

[9] Y. F. Chen and Y. P. Lan, "Dynamics of the Laguerre Gaussian $TEM_{0,l*}$ mode in a solid-state laser," *Phys. Rev. A*, vol. 63, no. 6, Jun. 2001, Art. no. 063807.

[10] J. Dong, J. Ma, Y. Y. Ren, G. Z. Xu, and A. A. Kaminskii, "Generation of Ince–Gaussian beams in highly efficient, nanosecond Cr,Nd:YAG microchip lasers," *Laser Phys. Lett.*, vol. 10, no. 8, Aug. 2013, Art. no. 085803.

[11] D. J. Kim and J. W. Kim, "High-power TEM_{00} and Laguerre-Gaussian mode generation in double resonator configuration," *Appl. Phys. B, Lasers Opt.*, vol. 121, no. 3, pp. 401–405, Dec. 2015.

[12] W. P. Kong, A. Sugita, and T. Taira, "Generation of Hermite-Gaussian modes and vortex arrays based on two-dimensional gain distribution controlled microchip laser," *Opt. Lett.*, vol. 37, no. 13, pp. 2661–2663, Jul. 2012.

[13] J. Dong, Y. He, X. Zhou, and S. C. Bai, "Highly efficient, versatile, self-Q-switched, high-repetition-rate microchip laser generating Ince–Gaussian modes for optical trapping," *Quantum Electron.*, vol. 46, no. 3, pp. 218–222, Mar. 2016.

[14] J. Dong, Y. He, S.-C. Bai, K.-i. Ueda, and A. A. Kaminskii, "A Cr^{4+}:YAG passively Q-switched $Nd:YVO_4$ microchip laser for controllable high-order Hermite–Gaussian modes," *Laser Phys.*, vol. 26, no. 9, Jul. 2016, Art. no. 095004.

[15] S. Han, Y. Q. Liu, F. Zhang, Y. Zhou, Z. P. Wang, and X. G. Xu, "Direct generation of subnanosecond Ince–Gaussian modes in microchip laser," *IEEE Photon. J.*, vol. 7, no. 1, Feb. 2015, Art. no. 4500206.

[16] S. Ngcobo, I. Litvin, L. Burger, and A. Forbes, "A digital laser for on-demand laser modes," *Nature Commun.*, vol. 4, Aug. 2013, Art. no. 2289.

[17] T. Sato, Y. Kozawa, and S. Sato, "Transverse-mode selective laser operation by unicursal fast-scanning pumping," *Opt. Lett.*, vol. 40, no. 14, pp. 3245–3248, Jul. 2015.

[18] J. Dong, S. C. Bai, S. H. Liu, K. I. Ueda, and A. A. Kaminskii, "A high repetition rate passively Q-switched microchip laser for controllable transverse laser modes," *J. Opt.*, vol. 18, no. 5, May 2016, Art. no. 055205.

[19] A. A. R. Alrashed and B. E. A. Saleh, "Decentered Gaussian beams," *Appl. Opt.*, vol. 34, no. 30, pp. 6819–6825, Oct. 1995.

[20] C. Palma, "Decentered Gaussian beams, ray bundles, and Bessel-Gauss beams," *Appl. Opt.*, vol. 36, no. 6, pp. 1116–1120, Feb. 1997.

[21] O. Svelto, *Principles of Lasers*, 5th ed., New York, NY, USA: Springer, 2010, pp. 131–137.

[22] C. Y. Li and J. Dong, "Pump beam waist-dependent pulse energy generation in $Nd:YAG/Cr^{4+}$:YAG passively Q-switched microchip laser," *J. Mod. Opt.*, vol. 63, no. 14, pp. 1323–1330, Feb. 2016.

[23] K. Yang, S. Z. Zhao, G. Q. Li, D. C. Li, and J. L. He, "Simple way to optimize the pulse duration of diode-pumped passively Q-switched laser," *Opt. Eng.*, vol. 47, no. 5, May 2008, Art. no. 054201.

[24] D. Naidoo, K. Aït-Ameur, M. Brunel, and A. Forbes, "Intra-cavity generation of superpositions of Laguerre–Gaussian beams," *Appl. Phys. B, Lasers Opt.*, vol. 106, no. 3, pp. 683–690, Mar. 2012.